NEUROSCIENCE

A hindbrain dopaminergic neural circuit prevents weight gain by reinforcing food satiation

Yong Han[1], Guobin Xia[1], Yanlin He[1†], Yang He[1], Monica Farias[1], Yong Xu[1,2], Qi Wu[1]*

The neural circuitry mechanism that underlies dopaminergic (DA) control of innate feeding behavior is largely uncharacterized. Here, we identified a subpopulation of DA neurons situated in the caudal ventral tegmental area (cVTA) directly innervating DRD1-expressing neurons within the lateral parabrachial nucleus (LPBN). This neural circuit potently suppresses food intake via enhanced satiation response. Notably, this cohort of DA^{cVTA} neurons is activated immediately before the cessation of each feeding bout. Acute inhibition of these DA neurons before bout termination substantially suppresses satiety and prolongs the consummatory feeding. Activation of postsynaptic $DRD1^{LPBN}$ neurons inhibits feeding, whereas genetic deletion of *Drd1* within the LPBN causes robust increase in food intake and subsequent weight gain. Furthermore, the $DRD1^{LPBN}$ signaling manifests the central mechanism in methylphenidate-induced hypophagia. In conclusion, our study illuminates a hindbrain DAergic circuit that controls feeding through dynamic regulation in satiety response and meal structure.

INTRODUCTION

Feeding, an evolutionarily conserved process key to survival, is orchestrated by multiplexed neural circuits in response to diverse peripheral signals (*1*–*3*). Feeding behavior is composed of appetitive feeding as characterized by seeking and approaching rewarding stimuli such as food and consummatory feeding involving meal initiation, engagement, and satiation (*4*, *5*). In particular, food satiation is a critical process that governs the size and termination of a meal (*6*, *7*). Peripheral signals such as cholecystokinin and glucagon-like peptide 1 elicit impact on satiation through the afferent vagus nerve that, in turn, excites neurons within the nucleus of the solitary tract (NTS) and parabrachial nucleus (PBN) of the hindbrain (*8*–*10*). While emerging evidence suggests that the satiety-defeating overeating fundamentally contributes to weight gain and obesity (*11*), the key neural circuits and neurotransmitter systems underlying food satiation remain poorly understood.

The PBN, previously known for relaying taste, somatosensory, and visceral signals to the forebrain, has an established critical role in control of feeding, glucose metabolism, and body weight (*12*–*17*). Some recent studies have shown that GABAergic projections from the hypothalamic agouti-related peptide (AgRP) neurons to the PBN are critical for transmitting hunger signals from the periphery (*15*). Acute ablation of AgRP neurons or genetic disruption of their GABA (γ-aminobutyric acid) biosynthesis leads to anorexia and severe weight loss (*18*, *19*). This lethal phenotype can be rescued by enhancing $GABA_AR$ signaling or by suppressing NMDAR (*N*-methyl-D-aspartate receptor) signaling within the PBN during a critical adaptation period (*15*, *16*). The PBN is innervated densely by the excitatory inputs from the NTS, which, in turns, receives serotonergic afferents from the caudal raphe nuclei, forming a circuitry that inhibits food intake (*20*). However, the circuitry mechanism as to how the PBN neurons are involved in food satiation is not yet known.

Emerging evidence shows that dopaminergic (DA) neurons located in the ventral tegmental area (VTA) are highly heterogeneous in both their anatomical localization and functional significance (*21*–*24*). Previous studies showed that the forebrain DA signaling system plays a role in the control of food reward and food-conditioned stereotypic behavior (*25*–*28*). However, intra–nucleus accumbens (Acb) infusion of either DRD1 agonist, DRD2 agonist, or DRD1/DRD2 antagonists fails to affect food intake (*29*), and DA depletion in the forebrain or within the Acb does not affect appetitive taste reactivity for food (*30*). Genetic inactivation of DA transporter or injection of amphetamine into the Acb, both resulting into DA release, fails to enhance appetitive response to sucrose (*31*, *32*). Chemogenetic activation of the mesolimbic VTA→Acb circuit does not affect total food intake (*33*). These studies implicate that the potential role of the forebrain DA signaling on innate feeding behavior and body weight control might be inadvertently masked or secondary to those stereotypic responses (*34*). On the other hand, the DRD1 signaling is distributed abundantly within the PBN, yet with no physiological role established (*35*, *36*). Systemic treatment of DRD1 agonist into mice has been shown to suppress the feeding of palatable diets (*37*, *38*), whereas pretreatment with a DRD1 antagonist was sufficient to block amphetamine-induced anorexia (*39*). Although these studies implicated an inhibitory role of DA in control of feeding, the mechanistic significance of the DAergic circuit in food satiation remains poorly understood (*4*, *34*, *40*).

In this study, we revealed the functional role of a previously unidentified DAergic neural circuit comprising of DA^{VTA} neurons and $DRD1^{LPBN}$ neurons on the control of consummatory feeding. We examined the neural activities of DA^{VTA} neurons during an integrated eating bout. We observed notably enhanced neural activities of DA^{VTA} neurons immediately before the bout termination. Genetic inhibition of these neurons prolonged the bout duration and led to an increase in food intake. We further showed that enhanced neural activities of $DRD1^{LPBN}$ neurons are associated with meal termination. Last, we tested and validated the hypothesis that methylphenidate (MPH)–induced hypophagia and weight loss were mediated by the $DRD1^{LPBN}$ signaling pathway. Our findings suggest that the neural circuit from DA^{VTA} neurons to $DRD1^{LPBN}$ neurons plays a critical role in the suppression of consummatory feeding by governing food satiation.

[1]USDA/ARS Children's Nutrition Research Center, Department of Pediatrics, Baylor College of Medicine, Houston, TX, USA. [2]Department of Molecular and Cellular Biology, Baylor College of Medicine, Houston, TX, USA.
*Corresponding author. Email: qiw@bcm.edu
†Present address: Brain Glycemic and Metabolism Control Department, Pennington Biomedical Research Center, Louisiana State University, Baton Rouge, LA 70808, USA.

RESULTS

We found that the DA^{VTA} axonal terminals were not only distributed in several forebrain structures such as the Acb but were also shown with high density within the lateral PBN (LPBN) (fig. S1). Using a viral retrograde-tracing technique (Fig. 1A), our results showed that ~50% of LPBN-projecting VTA neurons or Acb-projecting VTA neurons are DA neurons (Fig. 1, B to E, and fig. S2). Most of the VTA neurons projecting to the LPBN were located within the caudal VTA (cVTA), which shows that the VTA neurons projecting to the LPBN and Acb were two cohorts of nonoverlapping neurons (Fig. 1, C to G, and fig. S2). These results reveal the existence of a distinctive cVTA→LPBN neural circuit.

To examine the function of this neural circuit on controlling feeding, we performed optogenetic stimulation of DA^{VTA} axonal terminals within the LPBN and Acb by expressing channelrhodopsin (ChR2) in cVTA neurons and placing fiber-optic cannulae in the projection areas. Photostimulation of the $cVTA^{DA}$→LPBN circuit significantly suppressed fasting-induced intake of chow diet while locomotive activity remained intact (Fig. 1, H and J). In contrast, activation of the VTA^{DA}→Acb circuit significantly increased locomotive activity without affecting feeding (Fig. 1, I and J). To perform more precise manipulation of $DA^{VTA→LPBN}$ neurons, we used a combinatorial strategy (*41*) using retrograde *CAV-Flp*, which was injected into the LPBN coupled with *AAV9-C_{on}-F_{on}-ChR2-EYFP* injected into the cVTA of *Slc6a3^{Cre}* mice, permitting specific expression of ChR2 within $DA^{VTA→LPBN}$ neurons (Fig. 1K). In line with our retrograde-tracing study, we found that $DA^{VTA→LPBN}$ neurons expressing ChR2-EYFP were mainly located within the cVTA (Fig. 1, L and M). Optogenetic activation of these $DA^{cVTA→LPBN}$ neurons significantly decreased food intake after a fast, without affecting locomotive activity (Fig. 1, N and O), showing that a cohort of LPBN-projecting DA^{cVTA} neurons inhibits feeding.

To functionally delineate the $cVTA^{DA}$→LPBN neural circuit, we injected a combination of *AAV2-DIO-ChR2-GFP* and *AAV-CBA-DIO-WGA-ZsGreen* (transsynaptic tracer) into the cVTA of *Slc6a3^{Cre}* mice (*42*, *43*) to tag the LPBN neurons innervated by DA^{cVTA} neurons (Fig. 2, A and B). Patch-clamp recording revealed that $ZsGreen^{+}$ neurons within the LPBN received monosynaptic input from DA^{cVTA} axonal terminals (Fig. 2, C to E). Most $ZsGreen^{+}$ neurons (92.3%) were activated upon treatment of SKF81297, a selective DRD1 agonist (Fig. 2, F to H). Moreover, photostimulation of ChR2-expressing DA terminals depolarized ~67% of postsynaptic LPBN neurons in a reversible manner, which could be further blocked by the selective DRD1 antagonist SCH23390 (Fig. 2, I to K). There were ~37.5% of postsynaptic LPBN neurons recorded that did not respond to the DRD1 antagonist, suggesting the existence of other transmitter signaling pathways (e.g., glutamatergic). These electrophysiological results demonstrate a monosynaptic connection between DA^{cVTA} neurons and DRD1-expressing LPBN ($DRD1^{LPBN}$) neurons.

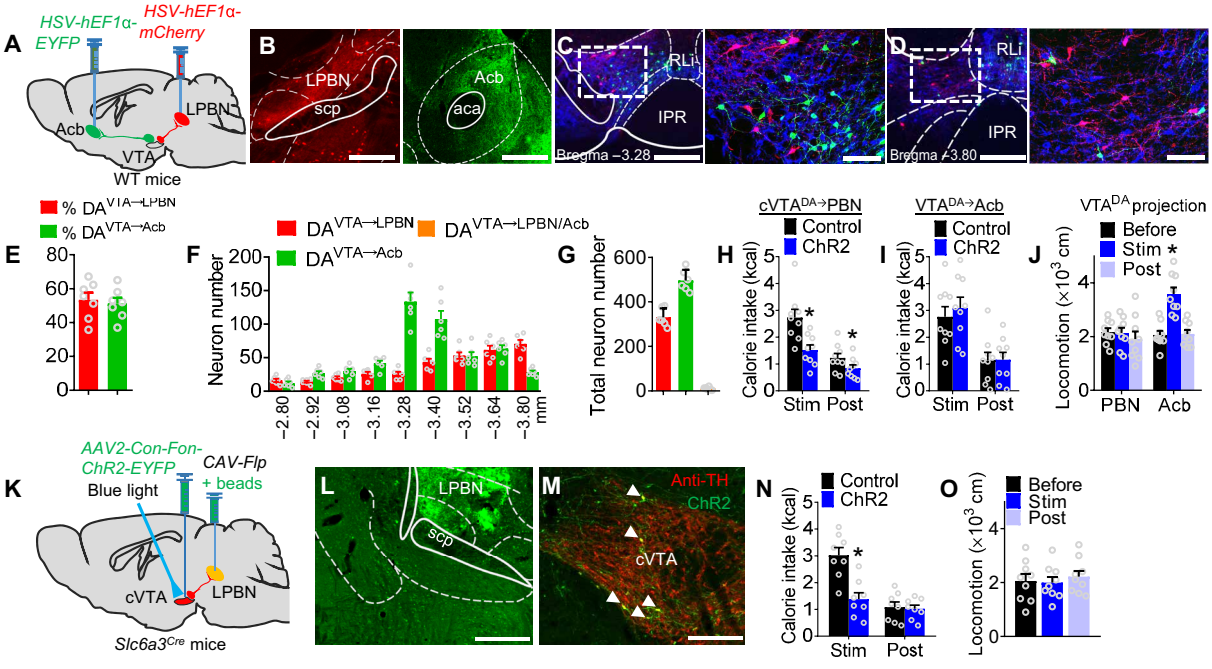

Fig. 1. A subset of DA neurons projecting from the cVTA to the LPBN neurons control food intake. (**A**) Diagram shows retrograde-targeting $DA^{VTA→LPBN}$ neurons and $DA^{VTA→Acb}$ neurons by unilateral injection of *HSV-hEF1α-mCherry* into the LPBN and *HSV-hEF1α-EYFP* into the Acb of WT mice. (**B**) The fluorescence in the local injection sites of LPBN and Acb. Scale bars, 200 μm. scp, superior cerebellar peduncle; aca, anterior commissure, anterior part. (**C** and **D**) Immunostaining of TH (blue) in the VTA. Scale bars (C and D), 200 μm (left) and 100 μm (right). IPR, interpeduncular nucleus, rostral subnucleus; RLi, rostral linear nucleus (midbrain). (**E**) Percentage of DA neurons ($n = 7$ per group). (**F**) Distribution of the DA neurons within unilateral VTA ($n = 6$ per group). (**G**) The total neuron number ($n = 6$ per group). (**H** to **J**) Refeeding and locomotion during and after 1 hour of photostimulation of DA terminals within the LPBN or Acb in *Slc6a3^{Cre}* mice with *AAV2-DIO-ChR2-GFP* virus into the VTA ($n = 9$ per group; $^{*}P < 0.05$). (**K**) Diagram showing injection of the mixture of *CAV-Flp* and carboxylate-modified fluorescent microspheres (to show the injection site) into the LPBN, followed by injection of *AAV9-C_{on}-F_{on}-ChR2-EYFP* within the cVTA of *Slc6a3^{Cre}* mice. (**L**) Injection site of *CAV-Flp* within the LPBN. Scale bar, 200 μm. (**M**) Retrograde-labeled ChR2 neurons (green) and anti-TH (red) within the cVTA. The arrowheads indicate the colocalization of ChR2 and TH. Scale bar, 200 μm. (**N** and **O**) Refeeding and locomotion during and after 1 hour of photostimulation of the cVTA ($n = 8$ per group; $^{*}P < 0.05$). Error bars represent means ± SEM. Two-way ANOVA followed by Bonferroni post hoc test in (H), (I), (N), and (O); Wilcoxon signed-rank test in (J).

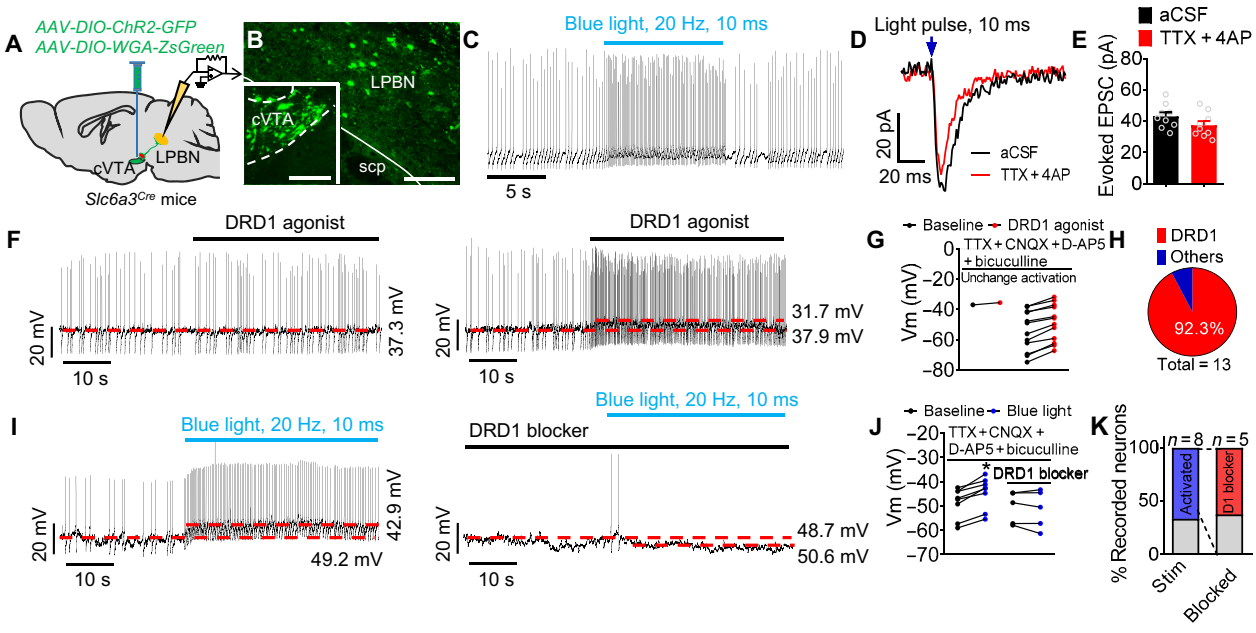

Fig. 2. A subpopulation of DA neurons in the VTA innervate DRD1 neurons in the LPBN. (**A**) Patch-clamp recording in GFP-labeled DRD1^{LPBN} neurons that are innervated by ChR2-expressing DA^{cVTA} neurons. *Slc6a3*^{Cre} mice were injected within the cVTA with *AAV2-DIO-ChR2-GFP* and *AAV-CBA-DIO-WGA-ZsGreen*. (**B**) Expression of GFP within the cVTA and LPBN. Scale bars, 150 μm. (**C**) Representative trace of LPBN neurons before and after photostimulation. (**D** and **E**) The response of EPSCs recorded from an LPBN neuron (D) and group data (E) upon photostimulation with or without pretreatment of TTX + 4AP. (**F** and **G**) Representative traces (F) and statistical analysis of membrane potential (Vm) (G) from LPBN neuron treated with SKF81297 ($n = 1$ in the unchanged group and $n = 12$ in the activation group. (**H**) Total neurons recorded in (G) (12 DRD1^{LPBN} neurons identified from 13 recorded neurons). (**I** and **J**) Representative traces (I) and statistical analysis of Vm (J) from LPBN neurons before and after photostimulation into the LPBN, without or with a pretreatment of SCH23390, a selective DRD1 antagonist ($n = 8$ in the optogenetic activated group and $n = 5$ in the DRD1 blocker group; $^*P < 0.05$; paired *t* test). (**K**) Percentage of recorded neurons depolarized by photostimulation in the presence of SCH23390. The blue-colored bar stands for the eight activated DRD1 neurons by photostimulation, and the red-colored bar stands for the five inhibited neurons by the DRD1 antagonist. Error bars represent means ± SEM.

We examined how DA^{cVTA} neurons contribute to a complete meal episode that was composed of eight or more feeding bouts (B1 to B8), whereby each feeding bout is composed of foraging (S1), prebout (S2), initiation (S3), engagement (S4), pretermination (S5), and interbout (S6) stages (fig. S3). Through optrode recording in vivo (Fig. 3A and fig. S4, A to C), putative DA neurons were identified by a basal firing rate of ≤10.0 Hz and spike width of ≥1.5 ms (fig. S4D) (*44*, *45*). We isolated ChR2-expressing DA^{cVTA} neurons that exhibited reliable light-evoked responses, indicating that these neurons projected to the LPBN (putative DA$^{cVTA→LPBN}$) (fig. S5) (*46*). The amount of food intake per each bout showed a gradual decrease from B1 to B8 in the first eight bouts of a meal (Fig. 3B). Meanwhile, the DA$^{cVTA→LPBN}$ neurons that were optogenetically activated, but not those that failed responding to photostimulation (i.e., DA$^{cVTA→Others}$ neurons), exhibited a progressive and significant increase in firing rate during S5 of each feeding bout that ultimately reached the peak level in B8 before the termination of a complete meal (Fig. 3, C to H). Thus, S5 was defined as a stage when the neural firing of DA$^{cVTA→LPBN}$ neurons rose to twofolds of the basic firing rate (Fig. 3G). Furthermore, statistical analyses of the spike rate indicated that putative DA$^{cVTA→LPBN}$ neurons displayed enhanced neuronal activity during S3 to S6 and a peak of activity (≥12 Hz) in S5 (Fig. 3I). The probability of termination of feeding was highly correlated with the duration of high-firing activity in S5, indicating that hyperactivity of putative DA$^{cVTA→LPBN}$ neurons during S5 was critical for meal cessation (Fig. 3J).

To further characterize the physiological role of DA$^{cVTA→LPBN}$ neurons in the context of meal cessation, we simultaneously treated *Slc6a3*^{Cre} mice with retrograde *CAV-Flp* injected into the LPBN and *AAV9-C*$_{on}$*-F*$_{on}$*-ChR2-EYFP* and *AAV9-C*$_{on}$*-F*$_{on}$*-NpHR3.3-EYFP* into the cVTA, thereby allowing expression of ChR2 and NpHR3.3 within DA$^{cVTA→LPBN}$ neurons (Fig. 3K). As before, DA$^{cVTA→LPBN}$ neurons were identified with the capacity to be photostimulated by ChR2 or photoinhibited by NpHR3.3 (fig. S6). To manipulate the activity of DA$^{cVTA→LPBN}$ neurons during the S5 stage, we programmed the pulse generator to exert photoinhibition based on the real-time monitor of firing rates from DA$^{cVTA→LPBN}$ neurons. To suppress the activity of DA$^{cVTA→LPBN}$ neurons during S5, the inhibitory opsin was activated in the cVTA 3 s after entering S5 (Fig. 3L). Optogenetic inhibition of DA$^{cVTA→LPBN}$ neurons during S5 significantly decreased the probability of meal termination and significantly prolonged bout duration (Fig. 3, M and N). The increase in food intake was strongly associated with the duration of optogenetic inhibition in S5 (Fig. 3O). These results demonstrate that the DA$^{cVTA→LPBN}$ neurons play a pivotal role in the control of the satiation response to food.

Infusion of the DRD1-selective agonists SKF38393 or SKF81297 into the LPBN suppressed food intake in mice after a fast (Fig. 4A and fig. S7). In contrast, administration of SKF81297 into the two brain regions close to the PBN, the laterodorsal tegmental nucleus (LDTg) or the supratrigeminal nucleus (Su5), had no effect on food intake (fig. S8). Chemogenetic activation of the DRD1^{LPBN} neurons by intraperitoneal injection of clozapine *N*-oxide (CNO)

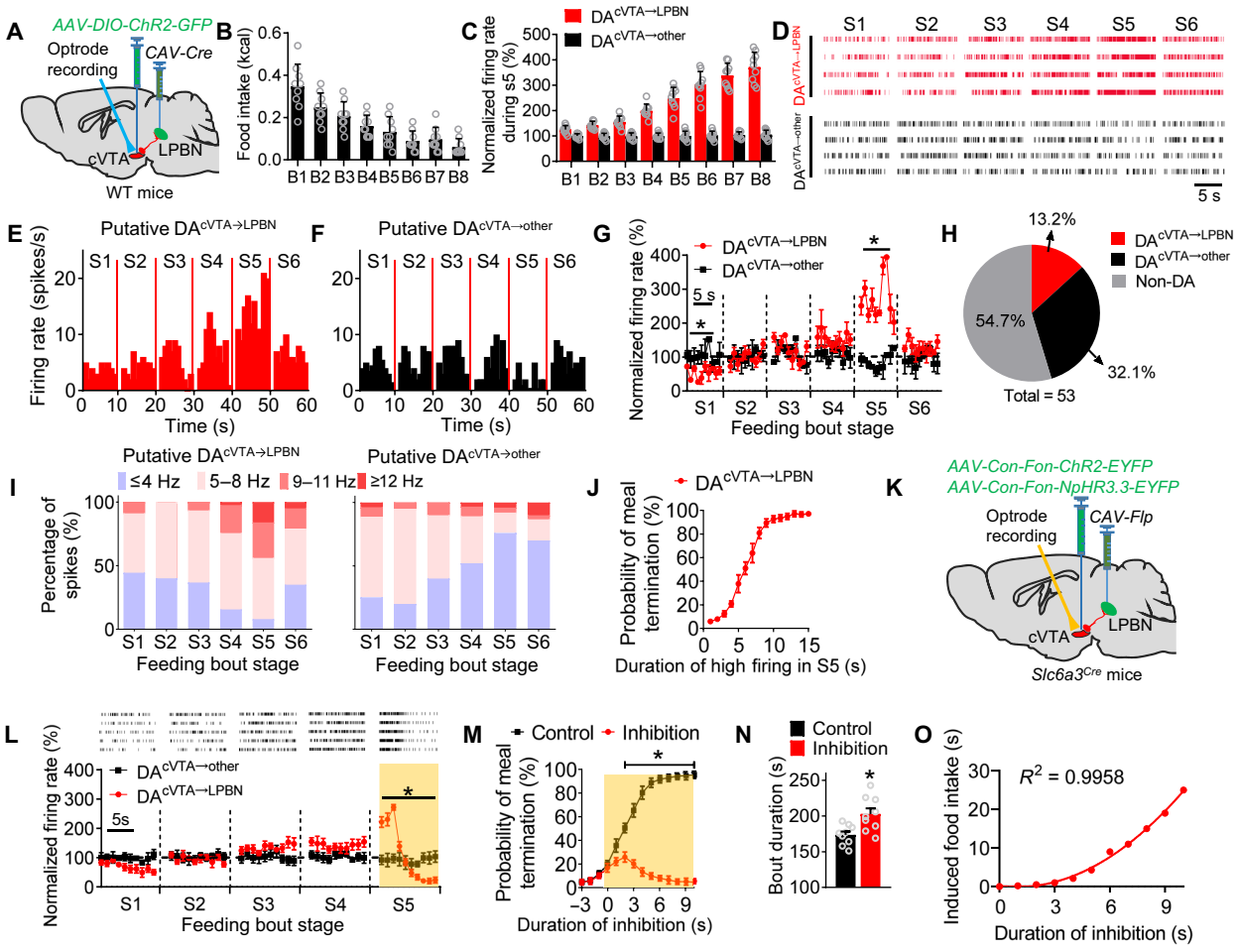

Fig. 3. The LPBN-projecting DA^{cVTA} neurons encode meal termination. (**A**) Optrode recording of VTA neurons projecting to the LPBN by injection of *CAV-Cre* into the LPBN, followed by *AAV2-DIO-ChR2-GFP* into the cVTA with the drive implantation above the cVTA. (**B**) Per bout food intake in meals composed of eight or more feeding bouts ($n = 9$ per group). (**C**) The normalized firing rate of putative DA neurons during S5 in each bout ($n = 9$ per group). (**D**) Representative firing raster from DA neurons during B8 in the isolated meals. (**E** to **G**) The firing rate and normalized firing rate of DA neurons during B8 in the isolated meals ($n = 7$ per group; $^*P < 0.05$). (**H**) The percentage of DA neurons in all recorded neurons (7 DA$^{cVTA→LPBN}$ neurons identified from 53 recorded neurons). (**I**) The distribution of spike numbers of DA neurons during B8. (**J**) The relationship between the probability of meal termination and duration of high-frequency firing of DA$^{cVTA→LPBN}$ neurons in S5. (**K**) Optrode recording of DA$^{cVTA→LPBN}$ neurons by injection of *CAV-Flp* into the LPBN, followed by injection of *AAV9-C$_{on}$-F$_{on}$-ChR2-EYFP* and *AAV9-C$_{on}$-F$_{on}$-NpHR3.3-EYFP* within the cVTA with the drive implantation above the cVTA of *Slc6a3^{Cre}* mice. (**L**) Representative firing raster (top) and normalized firing rate from seven DA$^{cVTA→LPBN}$ neurons and seven non–opto-tagged DA neurons. (**M**) The relationship between the probability of meal termination and duration of inhibition of DA$^{cVTA→LPBN}$ neurons in S5 of B8 ($n = 7$ per group; $^*P < 0.05$). (**N**) The bout duration under inhibition of DA$^{cVTA→LPBN}$ neurons in S5 ($n = 9$ per group; $^*P < 0.05$; unpaired *t* test). (**O**) The correlation analysis between induced food intake and duration of inhibition ($n = 6$ per group, nonlinear regression). Error bars represent means ± SEM. Two-way ANOVA followed by Bonferroni post hoc test was used in (E) to (G) and (M).

30 min before a feeding assay also reduced food intake after a fast (Fig. 4, B and C, and figs. S9 and S10), while chemogenetic silencing of DRD1^{LPBN} neurons enhanced food intake (Fig. 4D). These chemogenetic manipulations of DRD1^{LPBN} neuronal activity had no effect on locomotion activity (Fig. 4E).

To examine whether *Drd1* signaling contributes to feeding and body weight control, we inactivated the receptors by bilateral injection of *AAV2-CreGFP* into the LPBN of *Drd1$^{lox/lox}$* mice (Fig. 4F and fig. S11). This treatment led to a significant and progressive increase in food intake and body weight, without affecting locomotion (Fig. 4, G to J). Deletion of *Drd1* within the LPBN affected multiple aspects of consummatory feeding, including a significant increase in cumulative food intake, bout numbers, time in bouts and meals, and average meal size, without affecting meal numbers (Fig. 4, K to Q). These data reveal that DRD1^{LPBN} signaling regulates food intake through meal size and duration.

We investigated the real-time firing characteristics of DRD1^{LPBN} neurons in vivo throughout a complete feeding bout by expressing ChR2 in genetically identified DRD1 neurons and inserting an optrode. We isolated ChR2-expressing DRD1^{LPBN} neurons that exhibited reliable light-evoked responses, indicating that these neurons were DRD1^{LPBN} neurons (fig. S12). DRD1^{LPBN} neurons were activated by applying 20-Hz laser pulses, while non-DRD1 neurons were unaffected (Fig. 4R). Compared to other recorded LPBN neurons, the DRD1^{LPBN} neurons fired at significantly higher rates during S5, which is consistent with the peak activity of afferent DA$^{cVTA→LPBN}$ neurons during S5 (Fig. 4, S to V).

MPH is a clinically approved medication for the mitigation of attention deficit hyperactivity disorder (ADHD) and narcolepsy by

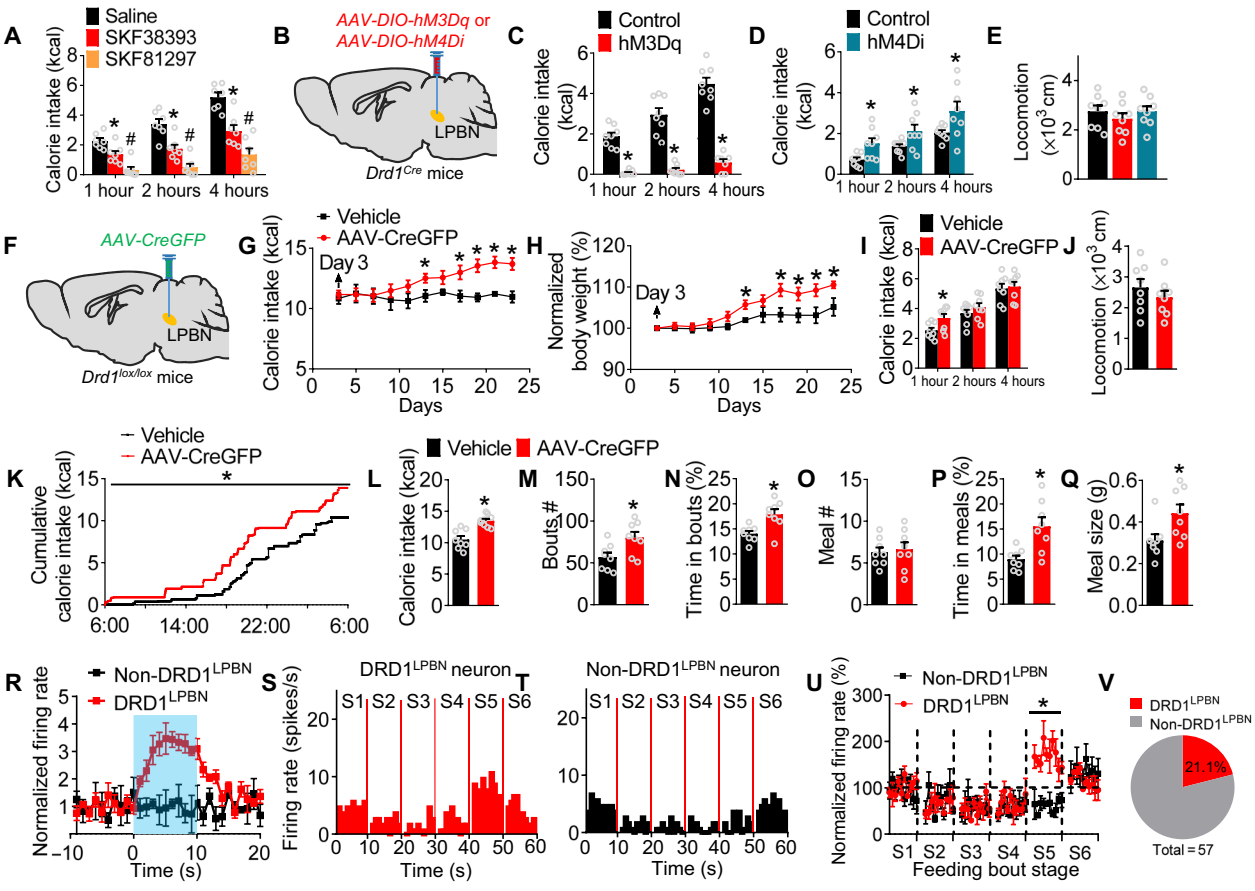

Fig. 4. The DRD1^{LPBN} signaling regulates consummatory feeding by increasing firing rate before meal cessation. (**A**) Refeeding test after bilateral infusion of the selective DRD1 agonist SKF38393 (1 μg per side) or SKF81297 (0.5 μg per side) into the LPBN ($n = 7$ per group; *$P < 0.05$, saline versus SKF38393; #$P < 0.05$, saline versus SKF81297; two-way ANOVA followed by Bonferroni post hoc test). (**B**) Chemogenetic manipulation of DRD1^{LPBN} neurons by injection of *AAV2-DIO-hM3Dq-mCherry* or *AAV2-DIO-hM4Di-mCherry* within the LPBN of *Drd1^{Cre}* mice. (**C** to **E**) Food intake and locomotion with CNO (0.1 mg/kg, ip) ($n = 8$ per group; *$P < 0.05$; two-way ANOVA followed by Bonferroni post hoc test). (**F**) Injection of *AAV2-CreGFP* within the LPBN of *Drd1$^{lox/lox}$* mice. (**G** to **J**) Food intake (G), body weight (H), refeeding (I), and locomotor activity (J) ($n = 8$ per group; *$P < 0.05$; two-way ANOVA followed by Bonferroni post hoc test). (**K** to **Q**) Cumulative food intake (K) and meal structure analysis (L to Q) [$n = 8$ per group; *$P < 0.05$; two-way ANOVA followed by Bonferroni post hoc test (K) and unpaired *t* test (L to Q)]. (**R**) Firing rate of representative DRD1 neurons in *Drd1^{Cre}* mice with an injection of *AAV2-DIO-ChR2-GFP* into the LPBN and implantation of optrode above the LPBN ($n = 12$ trials from 12 DRD1^{LPBN} neurons and $n = 15$ trials from 15 non-DRD1^{LPBN} neurons). (**S** to **U**) The firing rate and normalized firing rate of DRD1 neurons during B8 in the isolated meals [$n = 12$ per group in (U); *$P < 0.05$; two-way ANOVA followed by Bonferroni post hoc test]. (**V**) The percentage of DRD1^{LPBN} neurons and non-DRD1^{LPBN} neurons of all recorded neurons (12 DRD1^{LPBN} neurons identified from 57 recorded neurons). Error bars represent means ± SEM.

blocking dopamine and norepinephrine reuptake in the forebrain (*47*). The anorexigenic effect of MPH was notable in clinical studies, although there has yet to be any knowledge of its cellular targets or its underlying neural mechanism (*48*). To determine whether MPH regulates feeding through this cVTA→LPBN neural circuit, the LPBN-projecting VTA neurons were ablated by targeted expression of caspase-3 (fig. S13A). Immunostaining showed the DA$^{cVTA→LPBN}$ neurons were effectively ablated (fig. S13, B to D). Ablation of these neurons enhanced food intake and led to a 20% increase in body weight 4 weeks after viral transduction (Fig. 5, A to C). Administration of MPH caused a significant reduction in food intake and body weight, which was prevented by the ablation of VTA neurons projecting to the LPBN (Fig. 5, A to C). Consistently, chronic inactivation of the cVTA^{DA}→LPBN neural circuit abolished MPH-induced hypophagia and loss of body weight (Fig. 5, D to G). Genetic inactivation of *Drd1* within the LPBN abrogated MPH-induced hypophagia and weight loss in a progressive manner with an eventual reversion to hyperphagia and normalized body weight (Fig. 5, H to J). These results indicate that MPH suppresses feeding and causes weight loss by acting through this cVTA^{DA}→LPBN^{DRD1} pathway.

Electrophysiological recordings in vivo showed that MPH significantly increased the firing rate of DRD1^{LPBN} neurons throughout a feeding bout with the strongest elevation of firing rate in S5 as compared to non-DRD1^{LPBN} neurons (Fig. 5, K to M). These results indicate that the DA transmission onto the DRD1^{LPBN} neurons underlies the feeding and body weight control by MPH. Furthermore, microinjection of MPH into the PBN potently inhibited feeding on high-fat diet (HFD) and abolished HFD-induced obesity (Fig. 5, N to P). Together, these results suggest that MPH promotes a satiety response to HFD, thereby eliminating hyperphagia and obesity by augmenting DAergic transmission within the cVTA^{DA}→LPBN^{DRD1} circuit.

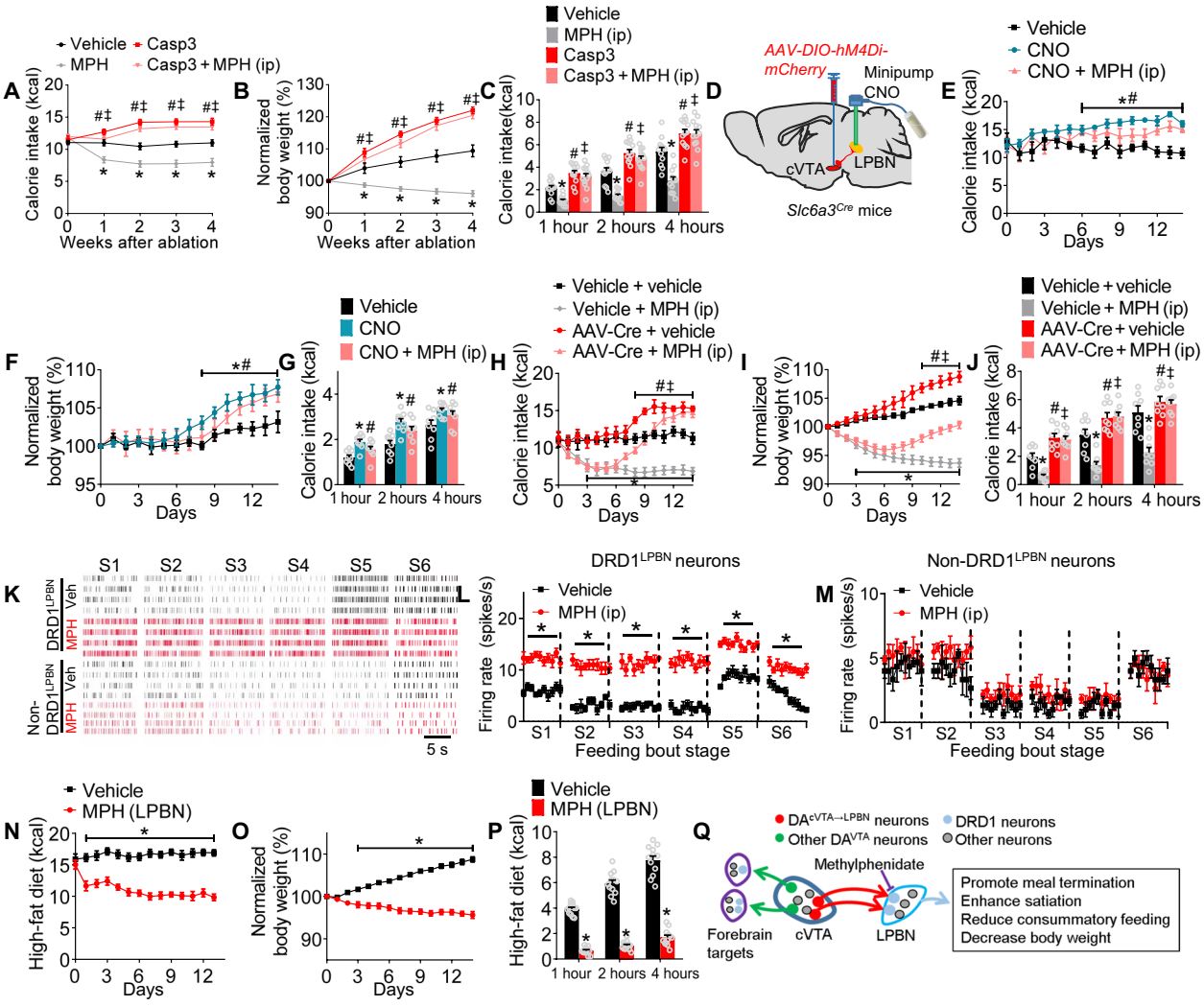

Fig. 5. MPH mediates hypophagia and body weight loss through the cVTA^{DA}→LPBN^{DRD1} circuit. (**A** to **C**) Food intake (A), body weight (B), and refeeding (C) with an injection of *CAV-Cre* into the LPBN and *AAV2-DIO-Casp3* into the cVTA with or without MPH (1.25 mg/kg, ip) ($n = 12$ per group; $^*P < 0.05$, vehicle versus MPH; $^\#P < 0.05$, vehicle versus Casp3; $^\ddagger P > 0.05$, Casp3 versus Casp3 + MPH). (**D**) Diagram showing chronic infusion of CNO into the LPBN by the osmotic minipump in *Slc6a3^{Cre}* mice after an injection of *AAV2-DIO-hM4Di-mCherry* into the cVTA with or without MPH (intraperitoneally). (**E** to **G**) Food intake (E), body weight (F), and feeding test in ad lib fed mice (G) ($n = 8$ per group; $^*P < 0.05$, vehicle versus CNO; $^\#P > 0.05$, CNO versus CNO + MPH). (**H** to **J**) Food intake (H), body weight (I), and refeeding test (J) with or without MPH (intraperitoneally) in *Drd1$^{lox/lox}$* mice with *AAV2-CreGFP* into the LPBN ($n = 8$ per group; $^*P < 0.05$, vehicle + vehicle versus vehicle + MPH; $^\#P < 0.05$, vehicle + vehicle versus AAV-Cre + vehicle; $^\ddagger P > 0.05$, AAV-Cre + vehicle versus AAV-Cre + MPH). (**K** to **M**) Representative firing raster (K) and firing rate (L and M) from DRD1 during B8 in the isolated meals by in vivo optrode-based recording with or without MPH (intraperitoneally) ($n = 12$ per group; $^*P < 0.05$). (**N** to **P**) Food intake (N), body weight (O), and refeeding test (P) with or without MPH into the LPBN in mice fed with HFD ($n = 12$ per group; $^*P < 0.05$). (**Q**) A subset of DA^{cVTA} neurons send DA projections to DRD1^{LPBN} neurons in the brainstem to reinforce meal satiety and reduce consummatory feeding, through which MPH exerts anti-obesity effects. Error bars represent means ± SEM. Two-way ANOVA followed by Bonferroni post hoc test was used in (A) to (C), (E) to (J), and (L) to (P).

DISCUSSION

Here, we showed that a subpopulation of DA neurons within the cVTA elicits precise control of bout duration and meal termination by acting through hindbrain DRD1^{LPBN} signaling (Fig. 5Q). Our present studies established that these DA^{VTA} neurons and their postsynaptic DRD1^{LPBN} neurons organize a functional neural circuit where DA$^{VTA→LPBN}$ neurons suppress consummatory feeding by showing robustly enhanced neural activities immediately before the termination of a feeding bout. Optogenetic inhibition of DA$^{VTA→LPBN}$ neurons is sufficient to decrease the probability of meal termination, prolong bout duration, and increase food intake. Consistently, postsynaptic DRD1^{LPBN} neurons suppress feeding by governing the meal termination response. In contrast to the CGRP^{PBN} neurons playing a role in control of adverse feeding (*12*), we demonstrated a previously unknown physiological role of DRD1^{LPBN} neurons in the regulation of the satiety response during consummatory feeding. Our results further suggested that the DRD1^{LPBN} signaling pathway centrally mediates the hypophagic effect of MPH. Overall, our study indicated that the cVTA^{DA}→LPBN^{DRD1} neural circuit, functionally segregated from other DA circuits, plays a pivotal

role in control of consummatory feeding by reinforcing the satiation response, thereby effectively reducing total food intake and body weight.

To reveal the anatomical structure of this DA circuit, we used a herpes simplex virus (HSV)–based retrograde-tracing method. Our results showed a total of ~500 $DA^{VTA→ACb}$ neurons in the unilateral side, which is consistent with a previous DA circuit mapping study (*49*). Comparably, we observed ~300 DA^{VTA} neurons in the unilateral side that sent projections to the LPBN, suggesting that $DA^{cVTA→LPBN}$ neurons account for a sizable population of the DA^{VTA} neurons. Furthermore, our results showed that most of the DA neurons that project to the PBN are located within the caudal region of the VTA. While the DA^{VTA} neurons do innervate D2R neurons in the Acb, our electrophysiological recording and behavioral data indicated that the D1R signaling within the VTA→PBN pathway contributes to the regulation of meal satiation and consummatory feeding (*50*, *51*). Although we observed that the LPBN neurons received direct, monosynaptic, DAergic innervations from the VTA, whether glutamate co-releases from DA^{VTA} neurons onto the PBN target neurons and whether the $glutamate^{VTA}$ signaling plays a role in control of meal satiation need further investigation. In our study, optogenetic activation of $DA^{VTA→LPBN}$ neurons was sufficient to suppress feeding but not affect locomotion, whereas activation of $DA^{VTA→ACb}$ neurons enhanced locomotion without obvious effects on feeding (*33*, *52*, *53*). These results suggest that the DA^{VTA} neurons projecting to the LPBN and ACb are anatomically and functionally segregated.

We detected notably enhanced activities of the $DA^{cVTA→LPBN}$ neurons in response to consummatory feeding. In our electrophysiological recording, we observed that more than 65% of meals contain eight or more feeding bouts. Hence, to reveal the significance of $DA^{cVTA→LPBN}$ neurons in contribution to the satiation response in a typical meal, the electrophysiological data from those meals that comprised of eight or more bouts were isolated. Our results showed that the firing rate in S5 was progressively increased from B1 and reached the peak level in the B8 (Fig. 3C). We further characterized the firing activities of DA^{cVTA} neurons (LPBN-projecting versus others) during B8 where each behaviorally defined feeding stage lasted no less than 10 s (Fig. 3, D to J). Nevertheless, the neuronal firing activities of this DAergic circuit in response to meals that contain either fewer than eight bouts or with any stage shorter than 10 s need further investigation. Our results strongly suggested that, for a typical meal, the $DA^{cVTA→LPBN}$ neurons exhibited obviously elevated activity before the meal termination. Moreover, optogenetic inhibition of $DA^{cVTA→LPBN}$ neurons resulted in a robustly reduced probability of meal termination. On the basis of these studies, we conclude that the LPBN-projecting DA neurons, but not other DA neurons, play a vital role in encoding meal satiation.

We functionally characterized a unique group of DRD1 neurons within the PBN. Chemogenetic activation of the $DRD1^{LPBN}$ neurons reduced food intake, while silencing of $DRD1^{LPBN}$ neurons played an exact opposite role. However, manipulation of $DRD1^{LPBN}$ neuronal activity had no effect on locomotion activity. Genetic deletion of *Drd1* signaling within the LPBN promoted food intake through robustly increasing meal size and duration. Electrophysiological recording results implicated that the $DRD1^{LPBN}$ neurons fired at significantly higher rates during the pretermination stage of the feeding bout. Therefore, we conclude that postsynaptic $DRD1^{LPBN}$ neurons play a role in DA^{VTA}-mediated control of food satiation. Clinical application of MPH in the treatment of ADHD reliably exhibits a reduced appetite and weight loss. We revealed that MPH suppresses feeding and body weight by strengthening the DAergic neural activity within the $cVTA^{DA}→LPBN^{DRD1}$ circuit, a new perspective that endorses a potential off-label application of a class of MPH and derivatives in tackling obesity and the future development of circuitry-based precision medicine that can deliver higher safety and effectiveness.

MATERIALS AND METHODS

Animals

All animal care and experimental procedures were approved by the Institutional Animal Care and Use Committees at Baylor College of Medicine (protocol #AN-6598). Mice used for data collection were at least 8 weeks old males and kept in temperature- and humidity-controlled rooms, in a 12-hour light/12-hour dark cycle, with lights on from 7:00 a.m. to 7:00 p.m. Health status was normal for all animals. $Slc6a3^{Cre}$ mice (stock no: 006660 in The Jackson Laboratory) (*54*), $Drd1^{Cre}$ mice (stock no: 37156-JAX in MMRRC) (*55*), and $Drd1^{lox/lox}$ mice (stock no: 025700 in The Jackson Laboratory) (*56*) were produced as previously described. All mice are on a C57Bl/6 background with at least eight generations backcrossed.

General surgical procedures

All the mice with brain surgery performed were provided the same preoperative and postoperative care. In all cases, for preoperative analgesia, buprenorphine (1.0 mg/kg, sc; 1 hour before the start of anesthesia) was administered. Animals were anesthetized with ~2% isoflurane anesthesia and placed on a stereotaxic frame (David Kopf, Tujunga, CA). A line block of local anesthetics (50/50 mix of lidocaine and bupivicaine in 1:20 dilution) (0.1 ml/25 g of mouse) was made before making an incision. For postoperative analgesia, buprenorphine (1.0 mg/kg, sc) was administered once 72 hours after surgery. All surgeries were performed having the animals placed on a heating pad and allowed to recover in a heating cage until they chose to reside in the unheated side of the cage.

Stereotaxic viral injections

After anesthetization, a circular craniotomy was drilled at the location per different experiments. In all experiments, virus was loaded into a needle (Hamilton Small Hub RN 33-gauge, Reno, NV) connected with a 10-μl syringe (Hamilton 700 Microliter, Reno, NV). Injections were performed with an Ultra MicroPump (World Precision Instruments, Sarasota, FL) and Micro4 controller (Heidenhain Corporation, Schaumburg, IL), at a rate of 0.1 μl/min. For adeno-associated virus (AAV), a total of 0.5-μl volume was delivered into brain regions. For CAV and HSV, a total of 0.2 μl was delivered into the LPBN or Acb. The relevant stereotaxic coordinates for the injections are described in the following according to a standardized atlas of the mouse brain (*57*). To target the cVTA, the coordinates used were as follows: anteroposterior (AP), −3.52 mm; mediolateral (ML), ±0.4 mm; dorsoventral (DV), −4.3 mm; the viral aliquots [*AAV2-hSyn-DIO-hM3D(Gq)-mCherry*, *AAV2-hSyn-DIO-hM4D(Gi)-mCherry*, and *AAV2-EF1a-DIO-hChR2(E123T/T159C)-GFP* from UNC were used and diluted to a final working titer of 7×10^{12} viral genomes/ml; *AAV9-Con-Fon-ChR2-EYFP* and *AAV9-Con-Fon-NpHR3.3-EYFP* were synthesized by GenScript, Piscataway, NJ, USA, and packaged by the Optogenetics and Viral Design/Expression

Core at Baylor College of Medicine and diluted to a final working titer of 3.6×10^{12} viral genomes/ml; *AAV9-DIO-WGA-zsGreen* was packaged by the Optogenetics and Viral Design/Expression Core at Baylor College of Medicine and diluted to a final working titer of 3.8×10^{12} viral genomes/ml; *AAV2-Flex-taCasp3-TEVP* from UNC was used and diluted to a final working titer of 1.8×10^{12} viral genomes/ml] were used for injection. To target the LPBN, the coordinates used were as follows: AP, −5.20 mm; ML, ±1.3 mm; DV, −3.4 mm; the viral aliquots [*CAV-Cre* and *CAV-Flp* from CNRS were used and diluted to a final working titer of 4.4×10^{12} and 9.3×10^{12} viral genomes/ml; *AAV2-hSyn-DIO-hM3D(Gq)-mCherry*, *AAV2-hSyn-DIO-hM4D(Gi)-mCherry; AAV2-GFP*, and *AAV2-CreGFP* were packaged by the Optogenetics and Viral Design/Expression Core at Baylor College of Medicine and diluted to a final working titer of 5×10^{12} viral genomes/ml; HSV hEF1α-mCherry from Harvard] were respectively injected. To target the Acb, the coordinates used were as follows: AP, +1.10 mm; ML, ±0.85 mm; DV, −4.6 mm; the viral aliquots (HSV hEF1α-EYFP from Harvard) were injected.

Double retrograde labeling

For the HSV tracing, HSV hEF1α-EYFP and HSV hEF1α-mCherry were unilaterally injected into the Acb and LPBN, respectively, in wild-type (WT) mice. The whole VTA, PBN, and Acb were sectioned with 20 μm thickness by a microtome (Thermo Fisher Scientific, Waltham, MA). The fluorescent images of green fluorescent protein (GFP) and mCherry neurons along the rostral to caudal axis of the VTA were obtained by an Axio Observer microscope (Zeiss, Thornwood, NY) and further analyzed using ImageJ software [National Institutes of Health (NIH)].

Ablation of DA^{cVTA} neurons projecting to the LPBN

To ablate DA^{cVTA} neurons, WT mice were bilaterally injected with *CAV-Cre* into the LPBN, and Cre-inducible AAV expressing caspase-3 (*AAV2-Flex-taCasp3-TEVP*) was injected within the cVTA. Twenty-eight days after injection, the mice were euthanized, and the brain was harvested. The whole VTA was sectioned with 20 μm thickness by a microtome (Thermo Fisher Scientific, Waltham, MA). Immunostaining for TH (tyrosine hydroxylase) was performed in all VTA sections. Fluorescent images of Cy3-labeled TH neurons along the rostral to caudal axis of the VTA were obtained by an Axio Observer microscope (Zeiss, Thornwood, NY) and further analyzed using ImageJ software (NIH) in which Abercrombie's correction of overcounting of profiles in sections was applied (*58*).

Optogenetics

For in vivo optogenetic stimulation, the optic fiber was assembled as described following the protocol (*59*). Briefly, the optical fiber (outer diameter, 250 μm; core diameter, 105 μm; numerical aperture, 0.22; FG105LCA, Thorlabs, Newton, NJ) was cut into small pieces (25 mm length) using a high-precision fiber cleaver (XL411, Thorlabs, Newton, NJ). The optical fiber was glued with a ceramic ferrule (inner diameter, 230 μm; Kientec System, Stuart, FL) and polished. To target the LPBN, the optical fiber was installed on the holder and guided into the coordinate (AP, −5.20 mm; ML, ±1.3 mm; DV, −3.2 mm). To target the Acb, the optical fiber was inserted with the following coordinates: AP, +1.1 mm; ML, ±0.85 mm; DV, −4.4 mm. To perform the photostimulation, the optical fiber was connected to Spectralynx (Neuralynx Inc., USA) through a patch cable. For the food intake measurement, the blue light was shed into the LPBN or Acb at 20 Hz with a 10-ms pulse for 1 hour. The power of laser (0.5 to 1.2 mW) was calculated by an optical power meter (PM100D, Thorlabs, Newton, NJ) before each experiment.

For in vitro optogenetics, an optical fiber (200 μm diameter) was coupled to a 473-nm solid-state laser diode. The fiber was passed through a stainless-steel tube (inner diameter, 250 μm; outer diameter, 480 μm) and bonded to the tube with glue. The tip of the fiber was trimmed and polished, submerged in artificial cerebrospinal fluid (aCSF), and placed above the LPBN. The blue light was controlled by a pulse stimulator. The blue light pulses (20 Hz, 10 ms per pulse) were shed onto the ChR2-expressing DA axonal fibers within the LPBN or ChR2-GFP–labeled LPBN neurons. The power of the laser (0.5 to 1.2 mW) was measured by a power meter (PM100D, Thorlabs, Newton, NJ) before experiments. To perform the photoinhibition, the optical fiber was connected to Spectralynx (Neuralynx Inc., USA) through a patch cable. The continuous yellow illumination (589 nm) was shed into the cVTA. The power of yellow light that we applied was 0.8 mW at the tip of the fiber, which was calculated by an optical power meter (PM100D, Thorlabs, Newton, NJ) before each experiment.

Drug administration

The mice received a general administration of CNO intraperitoneally at a dose of 0.1 mg/kg 30 min before feeding assay. The guide cannula (23-gauge steel, Plastics One) was used for infusing MPH, SFK38393, or SKF81297 into the LPBN or infusing SKF81297 into the LDTg or Su5. A circular craniotomy (diameter, 0.5 mm) was drilled at the locations of the LPBN, LDTg, or Su5. The guide cannula was installed on the holder and guided into the target brain region. To deliver the drug, the internal cannula was inserted onto the top of the guide cannula and extended below the guide cannula at 0.5 mm. To target the LPBN, the cannula was implanted within the LPBN with the following coordinates: AP, −5.2 mm; ML, ±1.3 mm; DV, −2.9 mm. To target the LDTg, the cannula was implanted within the LDTg with the following coordinates: AP, −5.02 mm; ML, ±0.7 mm; DV, −2.9 mm. To target the Su5, the cannula was implanted within the Su5 with the following coordinates: AP, −5.02 mm; ML, ±1.4 mm; DV, 4.0 mm. For some experiments, MPH (2 μg per side; Spectrum Chemical, New Brunswick, NJ), SKF38393 (1 μg per side; Tocris Bioscience, Minneapolis, MN), or SKF81297 (0.5 μg per side; Tocris Bioscience, Minneapolis, MN) was infused intracranially. For the experiments of systemic administration of MPH, the MPH was intraperitoneally injected with a dose of 1.25 mg/kg.

To chronically deliver CNO into the LPBN, a cannula was implanted within the LPBN, and an Alzet 14-day minipump (model 1002, Durect, Cupertino, CA) was used in this study. The minipump that dispensed at a speed of 0.25 μl/hour was loaded with 100 μl of CNO (0.12 μg/ml in saline; Enzo Life Sciences, Farmingdale, NY) and was implanted subcutaneously on the back of anesthetized mice for 14 days.

Food intake

For the acute feeding studies, food intake was measured (from the start of the "lights off" cycle, 6:00 p.m. to 7:00 p.m.) 1 hour during and after 1 hour of photostimulation with chow diet (5V5R, LabDiet, St. Louis, MO). For the refeeding test, food intake (1, 2, and 4 hours) was monitored from 12:00 p.m. to 4:00 p.m. with chow diet after 18 hours of fasting from 6:00 p.m. to 12:00 p.m. The food intake (1, 2, and 4 hours) in well-fed mice was monitored from 6:00 p.m.

to 10:00 p.m. with chow diet. The acute feeding and refeeding test were performed 3 weeks after virus injection. For the chronic feeding studies, food intake and body weight were measured daily between 9:00 a.m. and 10:00 a.m. for up to 4 weeks.

To study meal structure, the BioDAQ (Research Diets, NJ) was used 4 weeks after viral injection. Mice were habituated to BioDAQ cages for at least 10 days before feeding recordings. Feeding records were analyzed using BioDAQ Viewer (software v.2.3.07). A meal was defined if the food ingested in a bout feeding was ≥0.02 g and if it was separated from another meal by ≥5 min.

Feeding bouts were isolated by an interbout interval of 5 s, and meals consisted of one or more bouts separated by an intermeal interval of 5 min (*60*, *61*). A typical meal consists of ~8 bouts, and a single feeding bout is divided into six stages: foraging stage (S1); prebout stage (S2), 10 s before ingestion begins; initiation stage (S3), 10 s after ingestion begins; engagement stage (S4); pretermination stage (S5), 10 s before bout cessation; interbout stage (S6). The S1 to S6 stages were determined by the location of mice in the cage and the time spent in a specific arena (fig. S2B). The S1 to S6 stages (10 s per stage) were extracted from an integrated meal. The recording data from the bouts with all the stages lasting 10 s or more were extracted and binned to 10 s for presentation and statistical analysis, while those bouts with any of the stages lasting less than 10 s were discarded. An automated video-tracking system (EthoVision by Noldus) was used to track animals. Specifically, the home cage was divided into three arenas. The food was located on the middle of one side that was defined as a food zone. The size of the premeal zone (half circle, ~5 cm diameter) was adopted as half of the body length so as to match the center-point detection method. The reminder region in the home cage was defined as the foraging zone.

Measurement of locomotor activities

To assess locomotor activity, animals were gently removed from the home cage and placed singly into an open-field arena [Plexiglas cage, 50 cm (length) by 50 cm (width) by 40 cm (height)] 3 weeks after virus injection. An automated video-tracking system (EthoVision by Noldus) was used to track multiple subjects simultaneously. After the experiment, we gently returned each mouse to the respective home cage. To avoid olfactory cues, the arena (usually 50% ethanol) was carefully wiped after every running. The distance traveled within the chamber during a session of 5 min was calculated.

In vitro electrophysiology

The brains of adult mice were sectioned in coronal plane (250 to 300 μm). The brains and slices were handled and kept in aCSF as described recently (*62*). Animals were subjected to anesthesia, and the handling protocol of the local committee was followed. In most cases, we have used the same mouse first for the in vivo experiments and immediately after for combined electrophysiology and optogenetics in vitro to minimize the number of mice. Mice were deeply anesthetized with isoflurane and transcardially perfused with a modified ice-cold sucrose-based cutting solution (pH 7.3) containing 10 mM NaCl, 25 mM $NaHCO_3$, 195 mM sucrose, 5 mM glucose, 2.5 mM KCl, 1.25 mM sodium phosphate buffer, 2 mM Na-pyruvate, 0.5 mM $CaCl_2$, and 7 mM $MgCl_2$, bubbled continuously with 95% O_2 and 5% CO_2. The mice were then decapitated, and the entire brain was removed and immediately submerged in the cutting solution. Slices were cut with a Microm HM 650V vibratome (Thermo Fisher Scientific). Slices containing the PBN were recovered for 1 hour at 34°C and then maintained at room temperature (RT) in aCSF (pH 7.3) containing 126 mM NaCl, 2.5 mM KCl, 2.4 mM $CaCl_2$, 1.2 mM sodium phosphate buffer, 1.2 mM $MgCl_2$, 11.1 mM glucose, and 21.4 mM $NaHCO_3$, saturated with 95% O_2 and 5% CO_2 before recording. Slices were transferred to a recording chamber and allowed to equilibrate for at least 10 min before recording. The slices were superfused at 34°C in oxygenated aCSF at a flow rate of 1.8 to 2 ml/min. GFP- or mCherry-labeled neurons in the LPBN were visualized using epifluorescence and infrared differential interference contrast imaging on an upright microscope (Eclipse FN-1, Nikon) equipped with a moveable stage (MP-285, Sutter Instrument). Patch pipettes with resistances of 3 to 5 megohms were filled with intracellular solution (pH 7.3) containing 128 mM K-gluconate, 10 mM KCl, 10 mM Hepes, 0.1 mM EGTA, 2 mM $MgCl_2$, 0.05 mM Na-GTP, and 0.05 mM Mg-ATP. Recordings were made using a MultiClamp 700B amplifier (Axon Instruments), sampled using Digidata 1440A, and analyzed offline with pClamp 10.3 software (Axon Instruments). Series resistance was monitored during the recording, and the values were generally <10 megohms and were not compensated. The liquid junction potential was +12.5 mV and was corrected after the experiment. Data were excluded if the series resistance increased markedly during the experiment or without overshoot for action potential. Currents were amplified, filtered at 1 kHz, and digitized at 20 kHz. Current clamp was engaged to test neural firing frequency and resting membrane potential (Vm) at the baseline. The aCSF solution contained 1 μM tetrodotoxin (TTX) and a cocktail of fast synaptic inhibitors, AP-5 (30 μM; an NMDAR antagonist) and CNQX (30 μM; an AMPA receptor antagonist), to block most of the presynaptic inputs. For the light-evoked excitatory postsynaptic current (EPSC) recordings, the internal recording solution contained 125 mM $CsCH_3SO_3$, 10 mM CsCl, 5 mM NaCl, 2 mM $MgCl_2$, 1 mM EGTA, 10 mM Hepes, 5 mM (Mg)ATP, and 0.3 mM (Na)GTP (pH 7.3 with NaOH). mEPSC within the LPBN neurons was measured in the voltage clamp mode with a holding potential of −60 mV in the presence of 1 μM TTX and 50 μM bicuculline. 4AP (4-aminopyridine) and TTX were used to confirm the evoked EPSC currents are monosynaptic currents. Depolarization was defined as a >2-mV increase of the resting membrane potential, whereas hyperpolarization was defined as a >2-mV decrease of the resting membrane potential; values between a 2-mV decrease and a 2-mV increase were defined as "unchanged" (*63*).

In vivo tetrode recording

We used the microdrive model that enabled delivery of the laser or drug into the brain and recorded neural activities simultaneously (*64*, *65*). The microdrives were modified on the basis of tetrode microdrives from Neuralynx, which were loaded with one optic fiber in the center and seven nichrome tetrodes consisting of four thin wires twined together (Stablohm 675, California Fine Wire Co., Grover Beach, CA). The optic fiber was positioned 0.1 mm from the tetrode and was glued to the middle of the bundle of tetrodes. Tetrode tips were gold-plated to reduce impedance to 0.3 to 0.4 M (tested at 1 kHz). The microdrive was implanted into the cVTA in *Slc6a3*^{Cre} mice with an injection of *CAV-Flp* within the LPBN and an injection of *AAV-Con-Fon-ChR2-EYFP* and *AAV-Con-Fon-NpHR3.3-EYFP* within the cVTA. After recovery from microdrive implantation, the mouse was connected to a 32-channel preamplifier headstage. All signals recorded from each tetrode were amplified, filtered between 0.3 and 6 kHz, and digitized at 32 kHz. The local field potentials

were amplified and filtered between 0.1 Hz and 1 kHz. The tetrodes were slowly lowered in quarter turns of a screw on the microdrive (~60-μm steps). Spikes were sorted using Offline Sorter software (Plexon). Units were separated by the T-distribution E-M method, and cross-correlation and autocorrelation analyses were used to confirm unit separation. Clustered waveforms were subsequently analyzed by using NeuroExplorer (Nex Technologies, Colorado Springs, CO) or MATLAB (MathWorks, Natick, MA). The firing rates were presented with spikes per bin with 1-s intervals or spikes per second. Single units that had a basal firing rate of ≤10.0 Hz and spike width of ≥1.5 ms were assigned to the putative dopamine neurons (*44*, *45*). The $ChR2^+$ neurons were identified by the short latencies of evoked spikes accurately following high-frequency photostimulation, as well as the identical waveforms of evoked and spontaneous spikes (*66*).

According to our experimental data, the majority of the meals (>65%) recorded thus far by us contain eight or more feeding bouts, whereas a small number of meals contain few bouts. Thus, we isolated those meals comprised of eight or more feeding bouts for data analysis. The electrophysiological data derived from the first eight feeding bouts were analyzed to show the progressive increase of firing rate in S5 of bouts in the isolated meals. The firing activities during B8 in which each of the feeding stages lasts no less than 10 s were analyzed and presented, whereas data from the meals that contain either fewer than eight bouts or with any stage shorter than 10 s were excluded.

To inhibit the $DA^{cVTA\rightarrow LPBN}$ neurons during the S5 stage, the neural firing of $DA^{cVTA\rightarrow LPBN}$ neurons during feeding was continuously monitored, and the yellow light was given only when the firing increased to twofold of the basic firing rate and stayed for 3 s by real-time online firing rate analysis. To achieve an automatic, firing event–triggered photostimulation, we built a platform by integrating three major equipment, including the Digital Lynx SX recording system (Neuralynx), the RZ5P programmable real-time signal processor (Tucker-Davis Technologies), and the Spectralynx optogenetic box (Neuralynx). The analog outputs of the Digital Lynx SX were connected with onboard analog inputs of the RZ5P processor, while the BNC channel of the RZ5P was connected with the TTL I/O ports of the Spectralynx box. During a recording session, the sorted spike signals from $DA^{cVTA\rightarrow LPBN}$ neurons recorded by the Digital Lynx SX were fed to and processed by the RZ5P in a real-time manner under the control of Synapse Suite software (Tucker-Davis Technologies). In our experimental design, following upward crossing of the threshold for photoinhibition to twofold of the basic firing rate and staying for 3 s (during the S5) as preprogrammed in the Synapse Suite, the RZ5P generated and output a TTL signal to the Spectralynx optogenetic box and triggered laser stimulation (589 nm) for 10 s. The probability of meal termination, feeding bout duration, and food intake was calculated.

Histology

Immunostaining was performed as described with modification (*19*). Mice were euthanized and perfused transcardially with ice-cold phosphate-buffered saline buffer (pH 7.4) containing 3% (w/v) paraformaldehyde (Alfa Aesar) and 1% glutaraldehyde (Sigma-Aldrich, St. Louis, MO). Brains were collected and postfixed overnight under 4°C in a fixation buffer containing 3% paraformaldehyde. Free-floating sections (25 μm) were cut by a microtome (Thermo Fisher Scientific, Waltham, MA) and then blocked with 5% (w/v) normal donkey serum in 0.1% Triton X-100 [TBST buffer (pH 7.2)] for overnight. Rabbit anti-TH (1:1500 dilution; ABN60, EMD Millipore, Burlington, MA) was applied to the sections for overnight incubation under 4°C, followed by 4× 15-min rinses in the TBST buffer. Last, sections were incubated with Alexa Fluor Cy5-conjugated secondary antibody (1:1000 dilution; 711-175-152, Jackson ImmunoLab, West Grove, PA) or Alexa Fluor Cy3-conjugated secondary antibody (1:1000 dilution; 711-585-152, Jackson ImmunoLab, West Grove, PA) for 2 hours at RT, followed by 4× 15-min rinses in TBST buffer. For mounted sections, fluorescent images were captured by a digital camera mounted on an Axio Observer microscope (Zeiss, Thornwood, NY).

Fluorescence in situ hybridization (FISH) was performed to examine the expression of Drd1 in the LPBN. All reagents and the Drdr1 probe are commercially available from Advanced Cell Diagnostics (catalog no. 320293, Newark, CA). The RNAscope Fluorescent Assay is one of the FISH techniques to visualize cellular RNA targets in fresh-frozen tissues. All FISH procedures were performed following the protocol provided by the manufacturer. Briefly, fresh-frozen brain tissues were sectioned with a cryostat at 20 μm thickness and mounted onto SuperFrost Plus slides. Chilled slides were fixed with 4% paraformaldehyde for 15 min at 4°C. Then, the sections were dehydrated with grade ethanol. Slides were air-dried for 5 min at RT, and ~5 drops of RNAscope Protease IV were added to each section for 30 min at RT and then washed three times with PBN. The sections were hybridized with the Drd1 probe (catalog no. 461908, Advanced Cell Diagnostics) for 2 hours at 40°C. After two washes, the slides were hybridized with Amp1FL for 30 min, Amp-2FL for 15 min, Amp-3FL for 30 min, and Amp-4FL for 15 min at 40°C followed by washing three more times with PBN. Lastly, the glass covers were mounted onto glass slides. The fluorescent images were captured by an Axio Observer microscope.

Statistical analyses

Data were analyzed by unpaired *t* test, paired *t* test, and one-way or two-way analysis of variance (ANOVA) with appropriate post hoc testing. A Wilcoxon signed-rank test was used when the data were not normally distributed. Statistical analyses were performed using Prism software (GraphPad Software, San Diego, CA). Results were considered significantly different at $P < 0.05$. All data are presented as means ± SEM.

SUPPLEMENTARY MATERIALS

Supplementary material for this article is available at http://advances.sciencemag.org/cgi/content/full/7/22/eabf8719/DC1

View/request a protocol for this paper from *Bio-protocol*.

REFERENCES AND NOTES

1. C. J. Burnett, C. Li, E. Webber, E. Tsaousidou, S. Y. Xue, J. C. Brüning, M. J. Krashes, Hunger-driven motivational state competition. *Neuron* **92**, 187–201 (2016).
2. G. J. Morton, T. H. Meek, M. W. Schwartz, Neurobiology of food intake in health and disease. *Nat. Rev. Neurosci.* **15**, 367–378 (2014).
3. J. W. Sohn, J. K. Elmquist, K. W. Williams, Neuronal circuits that regulate feeding behavior and metabolism. *Trends Neurosci.* **36**, 504–512 (2013).
4. M. A. Rossi, G. D. Stuber, Overlapping brain circuits for homeostatic and hedonic feeding. *Cell Metab.* **27**, 42–56 (2018).
5. R. C. Ritter, Gastrointestinal mechanisms of satiation for food. *Physiol. Behav.* **81**, 249–273 (2004).
6. G. P. Smith, The direct and indirect controls of meal size. *Neurosci. Biobehav. Rev.* **20**, 41–46 (1996).
7. H. J. Grill, A role for GLP-1 in treating hyperphagia and obesity. *Endocrinology* **161**, bqaa093 (2020).

8. M. R. Hayes, L. Bradley, H. J. Grill, Endogenous hindbrain glucagon-like peptide-1 receptor activation contributes to the control of food intake by mediating gastric satiation signaling. *Endocrinology* **150**, 2654–2659 (2009).
9. G. L. Edwards, E. E. Ladenheim, R. C. Ritter, Dorsomedial hindbrain participation in cholecystokinin-induced satiety. *Am. J. Physiol.* **251**, R971–R977 (1986).
10. A. L. Alhadeff, J. P. Baird, J. C. Swick, M. R. Hayes, H. J. Grill, Glucagon-like peptide-1 receptor signaling in the lateral parabrachial nucleus contributes to the control of food intake and motivation to feed. *Neuropsychopharmacology* **39**, 2233–2243 (2014).
11. K. C. Berridge, 'Liking' and 'wanting' food rewards: Brain substrates and roles in eating disorders. *Physiol. Behav.* **97**, 537–550 (2009).
12. R. D. Palmiter, The parabrachial nucleus: CGRP neurons function as a general alarm. *Trends Neurosci.* **41**, 280–293 (2018).
13. R. Norgren, C. M. Leonard, Taste pathways in rat brainstem. *Science* **173**, 1136–1139 (1971).
14. J. F. Bernard, G. F. Huang, J. M. Besson, The parabrachial area: Electrophysiological evidence for an involvement in visceral nociceptive processes. *J. Neurophysiol.* **71**, 1646–1660 (1994).
15. Q. Wu, M. P. Boyle, R. D. Palmiter, Loss of GABAergic signaling by AgRP neurons to the parabrachial nucleus leads to starvation. *Cell* **137**, 1225–1234 (2009).
16. Q. Wu, M. S. Clark, R. D. Palmiter, Deciphering a neuronal circuit that mediates appetite. *Nature* **483**, 594–597 (2012).
17. S. M. Sternson, A. K. Eiselt, Three pillars for the neural control of appetite. *Annu. Rev. Physiol.* **79**, 401–423 (2017).
18. S. Luquet, F. A. Perez, T. S. Hnasko, R. D. Palmiter, NPY/AgRP neurons are essential for feeding in adult mice but can be ablated in neonates. *Science* **310**, 683–685 (2005).
19. F. Meng, Y. Han, D. Srisai, V. Belakhov, M. Farias, Y. Xu, R. D. Palmiter, T. Baasov, Q. Wu, New inducible genetic method reveals critical roles of GABA in the control of feeding and metabolism. *Proc. Natl. Acad. Sci. U.S.A.* **113**, 3645–3650 (2016).
20. Q. Wu, B. B. Whiddon, R. D. Palmiter, Ablation of neurons expressing agouti-related protein, but not melanin concentrating hormone, in leptin-deficient mice restores metabolic functions and fertility. *Proc. Natl. Acad. Sci. U.S.A.* **109**, 3155–3160 (2012).
21. J. Roeper, Dissecting the diversity of midbrain dopamine neurons. *Trends Neurosci.* **36**, 336–342 (2013).
22. M. Morales, E. B. Margolis, Ventral tegmental area: Cellular heterogeneity, connectivity and behaviour. *Nat. Rev. Neurosci.* **18**, 73–85 (2017).
23. S. Lammel, E. E. Steinberg, C. Földy, N. R. Wall, K. Beier, L. Luo, R. C. Malenka, Diversity of transgenic mouse models for selective targeting of midbrain dopamine neurons. *Neuron* **85**, 429–438 (2015).
24. M. J. Sanchez-Catalan, J. Kaufling, F. Georges, P. Veinante, M. Barrot, The antero-posterior heterogeneity of the ventral tegmental area. *Neuroscience* **282**, 198–216 (2014).
25. R. D. Palmiter, Dopamine signaling in the dorsal striatum is essential for motivated behaviors: Lessons from dopamine-deficient mice. *Ann. N. Y. Acad. Sci.* **1129**, 35–46 (2008).
26. A. Ilango, A. J. Kesner, K. L. Keller, G. D. Stuber, A. Bonci, S. Ikemoto, Similar roles of substantia nigra and ventral tegmental dopamine neurons in reward and aversion. *J. Neurosci.* **34**, 817–822 (2014).
27. H. C. Tsai, F. Zhang, A. Adamantidis, G. D. Stuber, A. Bonci, L. de Lecea, K. Deisseroth, Phasic firing in dopaminergic neurons is sufficient for behavioral conditioning. *Science* **324**, 1080–1084 (2009).
28. P. Xu, Y. He, X. Cao, L. Valencia-Torres, X. Yan, K. Saito, C. Wang, Y. Yang, A. Hinton Jr., L. Zhu, G. Shu, M. G. Myers Jr., Q. Wu, Q. Tong, L. K. Heisler, Y. Xu, Activation of serotonin 2C receptors in dopamine neurons inhibits binge-like eating in mice. *Biol. Psychiatry* **81**, 737–747 (2017).
29. B. A. Baldo, K. Sadeghian, A. M. Basso, A. E. Kelley, Effects of selective dopamine D1 or D2 receptor blockade within nucleus accumbens subregions on ingestive behavior and associated motor activity. *Behav. Brain Res.* **137**, 165–177 (2002).
30. B. A. Baldo, A. E. Kelley, Discrete neurochemical coding of distinguishable motivational processes: Insights from nucleus accumbens control of feeding. *Psychopharmacology* **191**, 439–459 (2007).
31. S. Pecina, B. Cagniard, K. C. Berridge, J. W. Aldridge, X. Zhuang, Hyperdopaminergic mutant mice have higher "wanting" but not "liking" for sweet rewards. *J. Neurosci.* **23**, 9395–9402 (2003).
32. K. S. Smith, K. C. Berridge, J. W. Aldridge, Disentangling pleasure from incentive salience and learning signals in brain reward circuitry. *Proc. Natl. Acad. Sci. U.S.A.* **108**, E255–E264 (2011).
33. L. Boekhoudt, T. J. M. Roelofs, J. W. de Jong, A. E. de Leeuw, M. C. M. Luijendijk, I. G. Wolterink-Donselaar, G. van der Plasse, R. A. H. Adan, Does activation of midbrain dopamine neurons promote or reduce feeding? *Int. J. Obes.* **41**, 1131–1140 (2017).
34. R. D. Palmiter, Is dopamine a physiologically relevant mediator of feeding behavior? *Trends Neurosci.* **30**, 375–381 (2007).
35. F. Sederholm, A. E. Johnson, U. Brodin, P. Sodersten, Dopamine D_2 receptors and ingestive behavior: Brainstem mediates inhibition of intraoral intake and accumbens mediates aversive taste behavior in male rats. *Psychopharmacology* **160**, 161–169 (2002).
36. S. Maltais, S. Côté, G. Drolet, P. Falardeau, Cellular colocalization of dopamine D1 mRNA and D2 receptor in rat brain using a D2 dopamine receptor specific polyclonal antibody. *Prog. Neuropsychopharmacol. Biol. Psychiatry* **24**, 1127–1149 (2000).
37. S. J. Cooper, H. A. Al-Naser, Dopaminergic control of food choice: Contrasting effects of SKF 38393 and quinpirole on high-palatability food preference in the rat. *Neuropharmacology* **50**, 953–963 (2006).
38. P. Terry, J. L. Katz, Differential antagonism of the effects of dopamine D1-receptor agonists on feeding behavior in the rat. *Psychopharmacology* **109**, 403–409 (1992).
39. T. Y. Chen, S. L. Duh, C. C. Huang, T. B. Lin, D. Y. Kuo, Evidence for the involvement of dopamine D_1 and D_2 receptors in mediating the decrease of food intake during repeated treatment with amphetamine. *J. Biomed. Sci.* **8**, 462–466 (2001).
40. C. M. Mazzone, J. Liang-Guallpa, C. Li, N. S. Wolcott, M. H. Boone, M. Southern, N. P. Kobzar, I. A. Salgado, D. M. Reddy, F. Sun, Y. Zhang, Y. Li, G. Cui, M. J. Krashes, High-fat food biases hypothalamic and mesolimbic expression of consummatory drives. *Nat. Neurosci.* **23**, 1253–1266 (2020).
41. J. F. Poulin, G. Caronia, C. Hofer, Q. Cui, B. Helm, C. Ramakrishnan, C. S. Chan, D. A. Dombeck, K. Deisseroth, R. Awatramani, Mapping projections of molecularly defined dopamine neuron subtypes using intersectional genetic approaches. *Nat. Neurosci.* **21**, 1260–1271 (2018).
42. D. Dautan, I. Huerta-Ocampo, I. B. Witten, K. Deisseroth, J. P. Bolam, T. Gerdjikov, J. Mena-Segovia, A major external source of cholinergic innervation of the striatum and nucleus accumbens originates in the brainstem. *J. Neurosci.* **34**, 4509–4518 (2014).
43. V. Gradinaru, F. Zhang, C. Ramakrishnan, J. Mattis, R. Prakash, I. Diester, I. Goshen, K. R. Thompson, K. Deisseroth, Molecular and cellular approaches for diversifying and extending optogenetics. *Cell* **141**, 154–165 (2010).
44. N. K. B. Totah, Y. Kim, B. Moghaddam, Distinct prestimulus and poststimulus activation of VTA neurons correlates with stimulus detection. *J. Neurophysiol.* **110**, 75–85 (2013).
45. T. Zhang, L. Zhang, Y. Liang, A. G. Siapas, F. M. Zhou, J. A. Dani, Dopamine signaling differences in the nucleus accumbens and dorsal striatum exploited by nicotine. *J. Neurosci.* **29**, 4035–4043 (2009).
46. J. Y. Cohen, S. Haesler, L. Vong, B. B. Lowell, N. Uchida, Neuron-type-specific signals for reward and punishment in the ventral tegmental area. *Nature* **482**, 85–88 (2012).
47. S. V. Faraone, E. J. Short, J. Biederman, R. L. Findling, C. Roe, M. J. Manos, Efficacy of Adderall and methylphenidate in attention deficit hyperactivity disorder: A drug-placebo and drug-drug response curve analysis of a naturalistic study. *Int. J. Neuropsychopharmacol.* **5**, 121–129 (2002).
48. C. Davis, L. Fattore, A. S. Kaplan, J. C. Carter, R. D. Levitan, J. L. Kennedy, The suppression of appetite and food consumption by methylphenidate: The moderating effects of gender and weight status in healthy adults. *Int. J. Neuropsychopharmacol.* **15**, 181–187 (2012).
49. S. Lammel, A. Hetzel, O. Häckel, I. Jones, B. Liss, J. Roeper, Unique properties of mesoprefrontal neurons within a dual mesocorticolimbic dopamine system. *Neuron* **57**, 760–773 (2008).
50. S. Ikemoto, B. S. Glazier, J. M. Murphy, W. J. McBride, Role of dopamine D_1 and D_2 receptors in the nucleus accumbens in mediating reward. *J. Neurosci.* **17**, 8580–8587 (1997).
51. E. E. Steinberg, J. R. Boivin, B. T. Saunders, I. B. Witten, K. Deisseroth, P. H. Janak, Positive reinforcement mediated by midbrain dopamine neurons requires D1 and D2 receptor activation in the nucleus accumbens. *PLOS ONE* **9**, e94771 (2014).
52. L. Boekhoudt, A. Omrani, M. C. M. Luijendijk, I. G. Wolterink-Donselaar, E. C. Wijbrans, G. van der Plasse, R. A. H. Adan, Chemogenetic activation of dopamine neurons in the ventral tegmental area, but not substantia nigra, induces hyperactivity in rats. *Eur. Neuropsychopharmacol.* **26**, 1784–1793 (2016).
53. A. J. Boender, J. W. de Jong, L. Boekhoudt, M. C. M. Luijendijk, G. van der Plasse, R. A. H. Adan, Combined use of the canine adenovirus-2 and DREADD-technology to activate specific neural pathways in vivo. *PLOS ONE* **9**, e95392 (2014).
54. C. M. Backman, N. Malik, Y. Zhang, L. Shan, A. Grinberg, B. J. Hoffer, H. Westphal, A. C. Tomac, Characterization of a mouse strain expressing Cre recombinase from the 3' untranslated region of the dopamine transporter locus. *Genesis* **44**, 383–390 (2006).
55. J. Zhang, L. Zhang, H. Jiao, Q. Zhang, D. Zhang, D. Lou, J. L. Katz, M. Xu, c-Fos facilitates the acquisition and extinction of cocaine-induced persistent changes. *J. Neurosci.* **26**, 13287–13296 (2006).
56. J. Sariñana, T. Kitamura, P. Künzler, L. Sultzman, S. Tonegawa, Differential roles of the dopamine 1-class receptors, D1R and D5R, in hippocampal dependent memory. *Proc. Natl. Acad. Sci. U.S.A.* **111**, 8245–8250 (2014).
57. K. B. L. Franklin, G. Paxinos, *The Mouse Brain in Stereotaxic Coordinates*, 3rd Edn. (San Diego CA: Academic Press, 2007).
58. M. Abercrombie, Estimation of nuclear population from microtome sections. *Anat. Rec.* **94**, 239–247 (1946).
59. F. Zhang, L. P. Wang, M. Brauner, J. F. Liewald, K. Kay, N. Watzke, P. G. Wood, E. Bamberg, G. Nagel, A. Gottschalk, K. Deisseroth, Multimodal fast optical interrogation of neural circuitry. *Nature* **446**, 633–639 (2007).

60. C. A. Campos, A. J. Bowen, M. W. Schwartz, R. D. Palmiter, Parabrachial CGRP neurons control meal termination. *Cell Metab.* **23**, 811–820 (2016).
61. A. Stengel, M. Goebel, L. Wang, J. Rivier, P. Kobelt, H. Mönnikes, Y. Taché, Activation of brain somatostatin 2 receptors stimulates feeding in mice: Analysis of food intake microstructure. *Physiol. Behav.* **101**, 614–622 (2010).
62. Y. He, G. Shu, Y. Yang, P. Xu, Y. Xia, C. Wang, K. Saito, A. Hinton Jr., X. Yan, C. Liu, Q. Wu, Q. Tong, Y. Xu, A small potassium current in AgRP/NPY neurons regulates feeding behavior and energy metabolism. *Cell Rep.* **17**, 1807–1818 (2016).
63. C. Duerrschmid, Y. He, C. Wang, C. Li, J. C. Bournat, C. Romere, P. K. Saha, M. E. Lee, K. J. Phillips, M. Jain, P. Jia, Z. Zhao, M. Farias, Q. Wu, D. M. Milewicz, V. R. Sutton, D. D. Moore, N. F. Butte, M. J. Krashes, Y. Xu, A. R. Chopra, Asprosin is a centrally acting orexigenic hormone. *Nat. Med.* **23**, 1444–1453 (2017).
64. P. Anikeeva, A. S. Andalman, I. Witten, M. Warden, I. Goshen, L. Grosenick, L. A. Gunaydin, L. M. Frank, K. Deisseroth, Optetrode: A multichannel readout for optogenetic control in freely moving mice. *Nat. Neurosci.* **15**, 163–170 (2012).
65. F. Liu, H. Jiang, W. Zhong, X. Wu, J. Luo, Changes in ensemble activity of hippocampus CA1 neurons induced by chronic morphine administration in freely behaving mice. *Neuroscience* **171**, 747–759 (2010).
66. D. Kvitsiani, S. Ranade, B. Hangya, H. Taniguchi, J. Z. Huang, A. Kepecs, Distinct behavioural and network correlates of two interneuron types in prefrontal cortex. *Nature* **498**, 363–366 (2013).

Acknowledgments: We appreciate the many helpful comments from R. Palmiter and colleagues at the University of Washington. We thank A. Del Favero-Campbell for editing of the manuscript. The *AAV-DIO-ChR2* backbone plasmid was a gift provided by S. Sternson (HHMI Janelia Research Campus). The *AAV-CBA-DIO-WGA-ZsGreen* vector was a gift provided by R. Palmiter. The Metabolomics Core and the Mouse Metabolism Core at Baylor College of Medicine provided various technical support. Some AAV vectors were packaged by the Optogenetics and Viral Design/Expression Core at Baylor College of Medicine. C. Ljungberg with the RNA In Situ Hybridization Core facility at Baylor College of Medicine provided technical support on the in situ hybridization. **Funding:** This project was supported by funding from a Shared Instrumentation grant from the NIH (S10 OD016167) and the NIH Digestive Diseases Center PHS grant P30 DK056338 to C. Ljungberg. This work was supported by NIH grants (R01DK109194 and R56DK109194) to Q.W., the Pew Charitable Trust awards to Q.W. (0026188), American Diabetes Association awards (#7-13-JF-61) to Q.W., Baylor Collaborative Faculty Research Investment Program grants to Q.W., USDA/CRIS grants (3092-5-001-059) to Q.W., the Faculty Start-up grants from USDA/ARS to Q.W., NIH grants (R01DK093587, R01DK101379, and R01DK117281) to Y.X., USDA/CRIS grants (3092-5-001-059) to Y.X., American Heart Association awards (17GRNT32960003) to Y.X., American Diabetes Association (1-17-PDF-138) to Yanlin He. Yanlin He is supported by the NIH Centers of Biomedical Research Excellence (COBRE) grant P20 GM135002. Q.W. is the Pew Scholar of Biomedical Sciences and the Kavli Scholar. **Author contributions:** Q.W. and Yong Han conceived and designed the experiments. Yong Han performed the surgery, in vivo electrophysiology, immunohistological imaging, and relevant data analysis. Yanlin He and Yang He performed slice electrophysiology. Yong Han and G.X. performed the behavioral tests and relevant data analysis. M.F. performed the colony management, genotyping, and some immunohistological assays. Q.W. and Yong Han wrote the manuscript with inputs from all authors on the manuscript. Y.X. provided comments for the manuscript. Q.W. supervised the project. **Competing interests:** The authors declare that they have no competing interests. **Data and materials availability:** All data needed to evaluate the conclusions in the paper are present in the paper and/or the Supplementary Materials. Additional data related to this paper may be requested from the authors.

Submitted 24 November 2020
Accepted 6 April 2021
Published 26 May 2021
10.1126/sciadv.abf8719

Citation: Y. Han, G. Xia, Y. He, Y. He, M. Farias, Y. Xu, Q. Wu, A hindbrain dopaminergic neural circuit prevents weight gain by reinforcing food satiation. *Sci. Adv.* **7**, eabf8719 (2021).